Atmos. Meas. Tech. Discuss., 5, 8051–8084, 2012
www.atmos-meas-tech-discuss.net/5/8051/2012/
doi:10.5194/amtd-5-8051-2012

Atmospheric Measurement Techniques Discussions

Depolarization ratio of Polar Stratospheric Clouds in coastal Antarctica: profiling comparison analysis between a ground-based Micro Pulse Lidar and the space-borne CALIOP

C. Córdoba-Jabonero[1], J. L. Guerrero-Rascado[2,3], D. Toledo[1], M. Parrondo[1], M. Yela[1], M. Gil[1], and H. A. Ochoa[4]

[1]Instituto Nacional de Técnica Aeroespacial (INTA), Atmospheric Research and Instrumentation Branch, Torrejón de Ardoz, 28850, Madrid, Spain
[2]Andalusian Center for Environmental Research (CEAMA), Group of Atmospheric Physics, Universidad de Granada-Gobierno Autónomo de Andalucía, Granada, Spain
[3]Universidad de Granada (UGR), Department of Applied Physics, Granada, Spain
[4]Dirección Nacional del Antártico/Instituto Antártico Argentino (DNA/IAA), Buenos Aires, Argentina

Received: 28 September 2012 – Accepted: 16 October 2012 – Published: 31 October 2012

Correspondence to: C. Córdoba-Jabonero (cordobajc@inta.es)

Published by Copernicus Publications on behalf of the European Geosciences Union.

AMTD

5, 8051–8084, 2012

Abstract

Polar Stratospheric Clouds (PSCs) play an important role in polar ozone depletion. In particular ice clouds, type PSC-II, with respect to the type PSC-I (nitric acid clouds) produce the most significant effects. Therefore PSC characterization, mainly focused on PSC-II discrimination is needed. The backscattering (R) and volume linear depolarization (δ^V) ratios are the parameters usually used in lidar measurements for PSC detection and identification. In this work, an improved version of the standard NASA/Micro Pulse Lidar (MPL-4), which includes a built-in depolarization detection module, has been used for PSC observations above the coastal Antarctic Belgrano II station (Argentina, 77.9° S 34.6° W, 256 m a.s.l.) since 2009. Examination of the MPL-4 δ^V feature as a suitable index for PSC-type discrimination is based on the analysis of the two-channel data, i.e. the parallel (p-) and perpendicular (s-) polarized MPL signals. This study focuses on the comparison of simultaneous δ^V-profiles as obtained from ground-based MPL-4 measurements during three Antarctic winters with those reported from the space-borne lidar CALIOP aboard the CALIPSO satellite in the same period (48 simultaneous cases are analysed for 2009–2011 austral winter times). Two different variables are considered for the comparison analysis between both lidar datasets in order to test the degree of agreement: the correlation coefficient (CC) and the percentage difference (BIAS). Results indicate a relatively good correlation between the δ^V-profiles once MPL-4 depolarization calibration parameters are applied. This correlation is based on the linear fitted height-range of the layered structure, obtaining CC values higher than 0.5 for 54 % (26 cases) out of all the analysed cases (48 in total). However, less satisfactory results are found when the BIAS test is used in the comparison procedure to test the degree of agreement between the lidar datasets. A predominance of negative BIAS values are observed showing that the MPL-4 δ^V values are underestimated with respect to CALIOP data; however, differences between the MPL-4 datasets are no greater than an 11 % (absolute value) with respect to CALIOP values. Moreover, the agreement appears to be unexpectedly independent of the CALIPSO ground-track

AMTD
5, 8051–8084, 2012

overpass distance from the Belgrano II station. Consequently, differences between the δ^V datasets are not dominated by spatial inhomogeneity of the PSC field.

1 Introduction

The polar stratosphere in both hemispheres is characterized by very low temperatures during winter leading to the formation of Polar Stratospheric Clouds (PSC). Heterogeneous chemical reactions occur on the surface of the PSCs, activating destructive compounds of ozone. Ozone destruction processes, through direct chlorine activation or indirectly through denitrification, are directly linked to the presence of a given type of PSC and influencing the degree of ozone depletion (Solomon, 1999). In Polar regions PSCs start to form during winter at stratospheric temperatures below the condensation threshold of the Nitric Acid Trihydrate (NAT), depending on the water vapour and nitric acid partial pressure (Hanson and Mauersberger, 1988). PSCs are classified in two groups depending on the temperature formation threshold (i.e. Toon et al., 1990): type I (PSC-I) are nitric acid clouds formed above the frost point (T_{NAT} = 194 K at 30 hPa), and type II (PSC-II) are water ice clouds (T_{ice} = 185 K at 30 hPa). Arctic temperatures are close to the threshold of PSC formation, hence both spatial and temporal PSC distributions present a high variability both in day to day and in year to year scales. In contrast, PSC presence in the Antarctica is almost ubiquitous from the beginning of wintertime to early springtime because of very low stratospheric temperatures extending over large areas. Indeed, Antarctic temperatures can reach rather lower values than Arctic temperatures (Parrondo et al., 2007), favouring a higher occurrence of PSCs over the Antarctic continent, including PSC-II clouds.

Due to the fact that non-spherical particles change the polarization state of the incident light, unlike spherical particles, PSCs can be detected and identified by using lidar systems with depolarization measurement capabilities. Lidar measurements have been widely used for PSC classification (PSC-I and PSC-II) on the basis of two lidar variables: the backscattering ratio (total backscatter-to-molecular coefficient ratio, R)

AMTD
5, 8051–8084, 2012

and the volume linear depolarization ratio (δ^V). Larger R and δ^V values are reported when PSC-IIs are present unlike PSC-Is and subtypes with smaller R and δ^V values from both ground-based (i.e. Adriani et al., 2004; Maturilli et al., 2005) and space-borne lidar observations (i.e. Pitts et al., 2009). PSC-Is and PSC-IIs have been detected in both hemispheres; however, the presence of PSC-IIs over the Southern Hemisphere is more persistent due to the fact that Antarctic temperatures usually can reach lower values than those in the Arctic, as result of a stronger and more stable Antarctic vortex during wintertime (Waugh and Polvani, 2010). Indeed, PSC-type identification is critical in polar ozone depletion research, and directly linked to stratospheric temperature variability.

The Instituto Nacional de Técnica Aeroespacial (INTA, Spain) in collaboration with the Dirección Nacional del Antártico/Instituto Antártico Argentino (DNA/IAA, Argentina) have been performing an extensive program for stratospheric ozone monitoring and research in Antarctica. One of the objectives was the climatology of high clouds in coastal Antarctica to link two highly-correlated fields: PSC formation and ozone depletion (Solomon, 1999). In the frame of the international Polar Year (IPY), an improved version of the standard NASA/Micro Pulse Lidar (MPL v.4, MPL-4, Sigma Space Corp.), which includes a built-in depolarization measurement module, is currently used for PSC observations in the Antarctic Belgrano II station (Argentina, 77.9° S 34.6° W, 256 m a.s.l.) since 2009. The column of air above this station remains well inside the polar vortex during wintertime (Parrondo et al., 2007), as shown in Fig. 1 in relation to the Antarctic polar vortex on 24 June 2010, providing thus an excellent location for PSC observations. Older versions than the MPL-4 have already been deployed in two other Antarctic stations (see Fig. 1): Syowa (Japan, 69.0° S 39.5° E), where a PSC type-II single event was reported and attributed to low temperature fluctuations related to inertia gravity waves (Shibata et al., 2003), and remaining usually outside the polar vortex (see Fig. 1); and South Pole/Amundsen-Scott (USA, 89.98° S 24.8° E), on the Antarctic Plateau (2835 m a.s.l.), where a 5-yr data record was obtained by using the noisier

AMTD
5, 8051–8084, 2012

MPL-3 with careful smoothing procedures (Campbell and Sassen, 2008). However, none of them include polarization measuring capabilities similar to those of the MPL-4.

A good performance of the MPL-4 system for PSC detection was previously achieved in the Arctic (Córdoba-Jabonero et al., 2009), where depolarization data confirmed that all the PSC cases detected during the 2006–2007 winter were related only to PSC-I events, and no PSC-II occurrences with larger δ^{V} values were found. Thus, the MPL-4 performance for discriminating Type I and Type II PSCs is still to be evaluated. A more detailed estimation of δ^{V} from MPL-4 measurements, based on the analysis of the two-channel data, i.e. both parallel (p-) and perpendicular (s-) polarization MPL signals, is examined in this work.

The space-borne lidar CALIOP on board the CALIPSO (Cloud-Aerosol Lidar and Infrared Pathfinder Satellite Observation, http://www-calipso.larc.nasa.gov) has provided valuable PSC information since 2006 at regional scales over both poles (Pitts et al., 2007, 2009, 2011). Therefore, MPL-4 depolarization retrievals are analyzed in comparison with the PSC volume linear depolarization ratio, δ^{V}, reported from the space-borne lidar CALIOP to test the degree of agreement between both datasets.

Both of the lidar systems and the depolarization data processing are described in Sect. 2. Section 3 presents results and discussion together with the analysis procedures applied to both δ^{V} datasets, where two different variables are considered for that analysis. Finally, the main conclusions are summarized in Sect. 4.

2 Instrumentation and methods

2.1 Lidar systems

2.1.1 Ground-based lidar: MPL-4

The Micro Pulse Lidar version 4 (MPL-4, Sigma Space Corp.) is an improved version of the standard Micro Pulse Lidar version 3 (MPL-3, SES Inc.) in routine operation within

AMTD
5, 8051–8084, 2012

the NASA/MPLNET (Micro-Pulse Lidar Network, http://mplnet.gsfc.nasa.gov) (Campbell et al., 2002). The MPL-4 system is configured in a zenith, monostatic, coaxial alignment and is based on an eye-safe pulsed Nd:YLF laser emitting at 527 nm with a high repetition-rate (2500 Hz) and low-energy (10 µJ, max.). Its receiver system consists of a Maksutov-Cassegrain 18 cm-diameter telescope, a birefrigent polarizer cell, and an avalanche photodiode detector. Backscattered signals are registered with a 1-min integration time and 75-m vertical resolution, commuting at each time the polarization module from parallel- to perpendicular-polarized detection (p- and s-channels, respectively). The system is able to probe the atmosphere up to 30 km with a sufficient signal-to-noise ratio. A full overlap is achieved at altitudes around 4 km up; however, the impact of the incomplete overlap effect on our retrievals is irrelevant because of: (i) its cancellation by δ^{V} is defined in this study (see Eq. 1 in Sect. 2.2), and (ii) PSCs usually appear at higher altitudes where a full overlap is achieved. The MPL-4 system is small, easy-to-handle with high autonomy and operational in full-time continuous mode. Hourly-averaged profiles are analyzed to study the spatial and temporal variability of the PSC distribution.

2.1.2 Space-borne lidar: CALIOP

The CALIPSO satellite carries the first space-borne lidar instrument CALIOP (Cloud-Aerosol Lidar with Orthogonal Polarization) which provides horizontally- (along the CALIPSO ground-track) and vertically-resolved measurements for aerosol and clouds distributions at a global scale. CALIOP is based on diode-pumped Nd:YAG laser emitting linearly polarized pulses with a repetition rate of 20.16 Hz and a pulse length of ∼ 20 ns, energy per pulse of 220 mJ at 1064 nm and ∼ 110 mJ at 532 nm. Its receiver system consists of a 1m-diameter telescope which feeds a three-channel receiver measuring the backscattered intensity at 1064 nm and the two orthogonal polarization components at 532 nm, parallel (p) and perpendicular (s). A full description of the CALIOP system can be found in Winker et al. (2007) and Hunt et al. (2009). CALIOP provides data at 532 nm (the closest wavelength to that of the MPL-4 system) with a different

AMTD
5, 8051–8084, 2012

vertical resolution as a function of altitude: 30 m at heights lower than 8.2 km, 60 m at 8.2–20.2 km, 180 m at 20.2–30.1 km, and 300 m at 30.1–40.0 km. In order to improve the signal-to-noise ratio, a horizontal averaging over 5 km CALIPSO ground-track and a vertical 7-point adjacent averaging are applied.

2.2 Depolarization data processing

The first lidar measurements of polarization properties were performed in the early 1970s (Schotland et al., 1971; Pal, 1973). It is well known that spherical particles do not change the polarization state of the incident light, while a partial depolarization component is introduced in the 180° backscattered signal after interacting with non-spherical particles. Several definitions are available in the lidar community to describe the depolarization phenomena caused by atmospheric constituents. A review of the most common parameters used in the lidar literature is given by Cairo et al. (1999). In our study, one of the most basic definitions is used, i.e. the volume linear depolarization ratio δ^{V} defined as follows:

$$\delta^{V}(z) = \frac{\beta^{\perp}(z)}{\beta^{\parallel}(z)} \tag{1}$$

where $\beta^{\perp}(z)$ and $\beta^{\parallel}(z)$ are the backscatter (particles plus molecules) coefficients for perpendicular- and parallel-polarization planes, respectively, and z is the height. In general, the term "particles" refers to both cloud and aerosol particles.

2.2.1 Ground-based depolarization measurements

From the practical point of view, the most general expression to calculate the volume linear depolarization ratio δ^{V} is:

$$\delta^{V}(z) = K\frac{P^{\perp}(z)}{P^{\parallel}(z)} + \chi \tag{2}$$

AMTD
5, 8051–8084, 2012

where $P^{\perp}(z)$ and $P^{\parallel}(z)$ are the s- and p-components of the measured MPL signals, respectively, once corrected for intrinsic instrumental factors (Campbell et al., 2002); K is a calibration constant that accounts for the differences of the receiver channel gains; and χ is a correction to account for any slight mismatch in the transmitter and detector polarization planes and any impurity of the laser polarization state (Sassen and Benson, 2001; Sassen, 2005). Because only a single detector is used in the MPL-4, the gain ratio is unity by definition and calibration requirements are vanished, however, at the expense of non-simultaneous measurements of the polarization components (see the review of existing techniques for estimating gain ratio in Álvarez et al., 2006). Fortunately, the impact of non-simultaneity on our retrievals is negligible due to the rather small PSC variability during the integration time (1 min) of each measurement. Thus, K is considered to be 1. The remaining correction term χ can be estimated by probing the δ^{V} values at middle and upper troposphere altitudes under both aerosol- and cloud-free conditions (calibration window, see Fig. 2). Optimal χ values are obtained by using fitting procedures with molecular backgrounds, considering a molecular volume linear depolarization ratio $\delta_{mol} = 0.0144$. Mean values of χ found for each year are presented in Table 1, showing a data dispersion of 5 % among these three years (a total of 778 hourly-averaged profiles were selected for that purpose). Those χ values are then used for calibration of the MPL-4 depolarization measurements following Eq. (2).

An example of this calibration approach performed on 1 July 2009 is illustrated in Fig. 2, where the volume linear depolarization ratio δ^{V} (left panel) together with the backscattering ratio R (centre panel) and the closest temperature profile provided from the local radiosounding (29 June 2009 at 11:00 UTC, right panel) are also represented. R, the total backscatter-to-molecular coefficient ratio (or the normalised R, $R_{norm} = 1 - 1/R$) usually used for PSC detection, is obtained by using a lidar ratio (extinction-to-backscatter coefficient ratio) of 30 sr in the Klett-Fernald inversion algorithm for backscatter coefficient retrieval (Klett, 1981; Fernald, 1984). A reference height is fixed when the condition of $R = 1$ ($R_{norm} = 0$, the strict case for an aerosol- and cloud-free molecular atmosphere) is found in the calibration window range considered.

AMTD
5, 8051–8084, 2012

On this particular day, a mean value of $\chi = -0.055 \pm 0.009$ is computed from the 24 daily profiles by using a calibration window from 5 to 7 km a.g.l. (grey band in Fig. 2). This value is similar to that reported for 2009 (see Table 1), which was applied to the 2009 winter dataset. Once the δ^V profile is calibrated, δ^V values larger than 0.2 are observed on 1 July 2009 at altitudes from 18.5 to 22 km and from 24 km height upwards, where a maximum $\delta^V = 0.5$ at 21–22 km height is identified (see Fig. 2, left), and $R \cong 10$ ($R_{norm} \cong 0.9$) is found (see Fig. 2, centre). This combination of R and δ^V values is typical for PSC-II events, as reported for several studies (i.e. Adriani et al. 2004; Maturilli et al. 2005; Pitts et al., 2009). This PSC-II feature is also confirmed by radiosonde data (see Fig. 2, right), reporting temperatures at those altitudes between 19.5 and 26.5 km height lower than the threshold for PSC-II formation, i.e. where $T < T^{PSC\text{-}II}$ (see Fig. 2, right panel, grey-shaded bands). A similar procedure is applied to all other uncalibrated MPL-4 δ^V profiles.

2.2.2 Space-borne depolarization measurements

CALIPSO provides Level 1, Level 2 and Level 3 products. Level 1 products include lidar calibrated and geo-located profiles of attenuated-backscatter coefficient at 1064 nm, and total and perpendicular-polarized attenuated backscatter coefficient at 532 nm. Level 2 products include cloud layer, aerosol layer and aerosol profiles at different horizontal resolutions. Level 3 products are monthly-averaged profiles of aerosol optical properties on a uniform grid in the tropospheric region for altitudes below 12 km height. A detailed description of products Levels 1 and 2 can be seen in Powell et al. (2010). The Level 1 V3-01 (version 3.01, validated stage 1) attenuated-backscatter profile products at 532 nm (total and perpendicular-polarized) are used in this study. The attenuated-backscatter coefficient profile is defined as the volume backscatter coefficient β multiplied by the two-way atmospheric transmission T^2 (Hostetler et al., 2006).

AMTD
5, 8051–8084, 2012

The total linear depolarization ratio δ_{total} is defined as:

$$\delta_{\text{total}}(z) = \frac{\beta^{\perp}(z)}{\beta^{\text{total}}(z)} \tag{3}$$

where $\beta^{\text{total}} = \beta^{\perp} + \beta^{\parallel}$, $\beta^{\perp}(z)$ and $\beta^{\parallel}(z)$ are the backscatter (particles and molecules) coefficients for s- and p-polarized components, respectively, and z is the range. Again, the term "particles" refers to both cloud and aerosol particles. For convenience, Eq. (3) can be multiplied by the term T^2, allowing for expressing the total linear depolarization ratio δ_{total} in terms of attenuated-backscatter coefficients:

$$\delta_{\text{total}}(z) = \frac{\beta^{\perp}(z)}{\beta^{\text{total}}(z)} = \frac{\beta^{\perp}(z)\cdot \mathrm{T}^2}{\beta^{\text{total}}(z)\cdot \mathrm{T}^2} = \frac{\beta^{\perp}_{\text{att}}(z)}{\beta^{\text{total}}_{\text{att}}(z)} \tag{4}$$

where $\beta^{\text{total}}_{\text{att}} = \beta^{\perp}_{\text{att}} + \beta^{\parallel}_{\text{att}}$, and $\beta^{\perp}_{\text{att}}(z)$ and $\beta^{\parallel}_{\text{att}}(z)$ are the attenuated-backscatter coefficient for s- and p-polarized components, respectively. $\beta^{\perp}_{\text{att}}$ and $\beta^{\text{total}}_{\text{att}}$ are provided by the CALIPSO Level 1 products. Finally, the δ_{total} values are converted into δ^{V} values using the following relationship (Cairo et al., 1999):

$$\delta^{\text{V}}(z) = \frac{\delta_{\text{total}}(z)}{1 - \delta_{\text{total}}(z)} \tag{5}$$

Therefore, the volume linear depolarization ratio δ^{V} can be compared between both MPL-4 and CALIOP datasets.

3 Results and discussion

3.1 Lidar datasets

PSC observations have been performed at the Belgrano II station since 2009 to the present. MPL-4 measurements for the 2009–2011 Antarctic winters, from May to

AMTD
5, 8051–8084, 2012

September, are used for this study. During these winter times, a total of 189 CALIPSO overpasses nearby the Belgrano II station were carried out within fewer 55 km distance between the satellite ground-track and the station. Among them, 104 overpasses are coincident events with MPL-4 measurements reporting PSC detection and 48 of them are available for comparison at the same time. The date and time, together with the ground-track distance of the CALIPSO overpass closest to the station for all these PSC cases, are shown in Table 2.

These coincident datasets are used for comparison analysis, where hourly-averaged MPL-4 profiles around each time period are used instead of the instantaneous 1-min profiles for that simultaneous time. This improves the signal-to-noise ratio of lidar measurements at Belgrano II station. A height-interval from 5 to 30 km is selected for the comparison between lidar profiles. A delineating altitude of 10 km has been conservatively established as the lower limit for the unambiguous presence of PSCs, distinguishing them from other upper tropospheric clouds (mainly Cirrus clouds). The lower limit of 10 km chosen in this work for PSC detection is based on the fact that the tropopause is not clearly delineated by the temperature profile during wintertime in deep Antarctica (Rubin, 1953). Indeed, a traditional tropopause height, denoted by rapidly increasing static stability above it, can be approximated from December through March in Belgrano II station sounding data around 9 km. During winter months, however, temperatures decrease with height to nearly 23 km. Dynamic coupling between the troposphere and stratosphere is more likely in such conditions. The region from 8 to 10 km is considered a transitional zone, where cloud type cannot be established with any certainty.

Although our study is restricted to PSC formation altitudes, the 5–10 km height interval is also considered for contrast as a PSC-free region. Heights above 30 km are disregarded due to decreased MPL-4 signal-to-noise ratio. In addition, negative δ^{V} values are disregarded for both datasets. Finally, along the overall height-range selected, every 0.5-km layer is averaged for comparing the MPL-4 and CALIOP datasets.

AMTD
5, 8051–8084, 2012

3.2 Comparison analysis

Two approaches are used for comparison analysis:

1. Calculation of the correlation coefficient (CC) between the two lidar measurements, and
2. the percentage difference, BIAS(z), between both MPL-4 and CALIOP δ^{V} profiles, defined as:

$$\mathrm{BIAS}(z) = \frac{100 \times \left[\delta^{\mathrm{MPL}}(z) - \delta^{\mathrm{CAL}}(z)\right]}{\delta^{\mathrm{CAL}}(z)} \quad (6)$$

where $\delta^{\mathrm{MPL}}(z)$ is the 0.5-km averaged MPL-4 volume linear depolarization ratio profile, and $\delta^{\mathrm{CAL}}(z)$ is the same but for CALIOP.

3.2.1 Comparison analysis I: Linear regression and correlation coefficient (CC)

The correlation coefficient, for the 0.5-km averaged profiles, was calculated for 48 cases over the total altitude range (see Table 2). This analysis is also performed as a function of different altitude intervals in order to examine similarities and/or discrepancies between different PSC layers as observed by both MPL-4 and CALIOP in each case. This procedure can reveal the degree of agreement between both datasets as a function of height. Five altitude intervals are selected: 5–10 km, 5–15 km, 5–20 km, 5–25 km and 5–30 km. Table 3 summarizes the results. They are based on the significance of these correlation coefficients obtained. Therefore, a value of CC = 0.5 is considered statistically significant depending on the number of data points deemed into the calculation, where a p-value less than the chosen significance level (α) of 0.05 must be reported. In this sense, for the particular case of a height interval of 5–15 km with a smaller number of data points than that for other height intervals considered in this study, a test statistic t = 2.09 and CC = 0.46 are calculated reporting p-values

AMTD
5, 8051–8084, 2012

lower than 0.05. Consequently, for other height intervals with larger number of data points, p-values must be also lower than α, and therefore those obtained CC can be regarded as statistically significant in this study.

In 2009, the largest CC values are found for the 5–25 km height interval, when 8 out of the total 15 cases present CC values higher than 0.5, representing a 53 % out of the cases for 2009 (see Table 3). In particular, 4 out of those cases show CC > 0.7 (29 and 30 June, and 1 and 30 July); and other 4 cases present CC in the interval 0.5–0.7 (31 July, 1 and 25 August, and 28 September). Slightly smaller correlations are found in 2010, when 9 out of the total 18 cases show CC values higher than 0.5, i.e. 50 % out of the cases in 2010, and within a lower correlation fitting range (5–20 km, see Table 3). In particular, three cases with CC values higher than 0.7 are found (24 and 25 June, and 28 August). Six other cases present CC within the 0.5–0.7 interval (8, 9 and 11 June, 2 and 13 July, and 27 August). In 2011, the situation is slightly better, being the best correlation fitting range of 5–20 km as in 2010, with a 60 % out of the cases (9 out of 15) presenting CC values higher than 0.5. Among them, 3 cases show CC > 0.7 (7 and 30 July, and 23 August) and six other cases (29 May, 6 and 29 July, and 14, 21 and 24 August) with CC values in the 0.5–0.7 interval (see Table 3).

In general, among the 48 MPL-4/CALIOP profile coincidences examined in total, 26 out of them (54 %) present CC values higher than 0.5, at least in the correlation fitting height-range of 5–20 km (see Table 3). That correlation becomes relatively worse when altitudes higher than 25 km are considered. However, PSC formation occurs indeed more frequently at altitudes lower those heights. Therefore, these results represent a relatively good agreement for the PSC volume linear depolarization ratio δ^{V} between MPL-4 and CALIOP profiles.

Moreover, in order to check the correlation dependence on the distance of the CALIPSO overpass from Belgrano II station, CC values are represented in Fig. 3 as a function of three predominant distance-ranges (0–10 km, 20–30 km and 45–55 km, shown by grey bands in Fig. 3) for each year. Results show unexpectedly a clear independence on that distance for all the years, and indeed no improvement is observed in

AMTD
5, 8051–8084, 2012

the correlation coefficient when the CALIPSO ground-track is just at a few kilometres (0–10 km) from the station (see Fig. 3). This apparent discrepancy indicates that differences between both the datasets are not dominated by spatial inhomogeneity of the PSC field.

3.2.2 Comparison analysis II: Percentage differences (BIAS)

This procedure has previously been used for ground-based lidar profiles in comparison with CALIOP data for the case of the tropospheric attenuated backscatter coefficients at middle-latitude regions (Mamouri et al., 2009; Mona et al., 2009). However, this same lidar profile comparison procedure, as focused on the PSC volume linear depolarization ratio δ^{V}, is for the first time applied in this work. Both 0.5-km averaged MPL-4 and CALIOP datasets are used to calculate the BIAS (see Eq. 6) in each case, as an altitude-dependent parameter obtained for comparison analysis between both lidar datasets.

Due to the large BIAS data dispersion obtained in general, a constraint condition ($-50\,\% < \mathrm{BIAS} < +50\,\%$) is applied to the BIAS profiles. From a statistical point of view, a height-averaged BIAS, $\langle \mathrm{BIAS}_z \rangle$, is calculated from the "constrained" profiles, with respect to the number of data points in each profile fulfilling that condition. In principle, a total of 50 data points are in the range from 5 to 30 km height for 0.5-km averaged profiles. However, no points in a given range can exist for any of both datasets since negative δ^{V} values are disregarded (see Sect. 2.3). Therefore the total "valid" data points (N, with no negative δ^{V} values) in a profile can be less than 50, and only those "valid" BIAS values are considered in analysis calculations. "Constrained" $\langle \mathrm{BIAS}_z \rangle$ values as obtained by this procedure for all the cases are shown in Table 4 together with their standard deviation (SD), including the percentage of number of data points fulfilling that condition (N^{BIAS}, in % respect to N) for each case.

In order to examine the BIAS in each overall time period, the "constrained" BIAS is also averaged for each year, $\langle \mathrm{BIAS}_t \rangle$, whereby a mean value of the data points $\langle N^{\mathrm{BIAS}} \rangle$

AMTD
5, 8051–8084, 2012

(in %) fulfilling the constraint condition applied is also obtained for each period. In particular, $\langle \mathrm{BIAS}_t \rangle$ values of $-7 \pm 8\,\%$ ($\langle N^{\mathrm{BIAS}} \rangle = 34 \pm 8\,\%$ of total "valid" data points N), $-6 \pm 8\,\%$ ($\langle N^{\mathrm{BIAS}} \rangle = 36 \pm 14\,\%$) and $-11 \pm 9\,\%$ ($\langle N^{\mathrm{BIAS}} \rangle = 43 \pm 15\,\%$) are found for 2009 (15 cases), 2010 (18 cases) and 2011 (15 cases), respectively. These results show that less than a half of the cases fulfil the constraint ($-50\,\% < \mathrm{BIAS} < +50\,\%$) condition, showing thus a large data dispersion with BIAS values higher than $\pm 50\,\%$. Despite these results, differences between δ^{MPL} and δ^{CAL} are no higher than an 11 % (absolute value) respect to CALIOP values in the worse case (in 2011), being in general δ^{MPL} underestimated with a clear predominance of negative $\langle \mathrm{BIAS}_t \rangle$ values (see Table 4). It is worth mentioning that the calculated percentage differences, BIAS, are rather large at PSC-free altitudes, mostly in the 5–10 km height-range, due to relatively low δ^{CAL} values close to the molecular one ($\delta_{\mathrm{mol}} = 0.0144$) in that region, and BIAS consequently increases following Eq. (6).

As for the correlation coefficient (see Sect. 3.1), the BIAS dependence on the CALIPSO ground-track distance from Belgrano II station is also checked. BIAS values obtained for each year as a function of those three main distance-ranges (0–10 km, 20–30 km and 45–55 km) are shown in Fig. 4. A predominance of negative values is observed, showing the previously observed δ^{MPL} underestimation respect to δ^{CAL}. In particular, averaged BIAS on those three distance-ranges, $\langle \mathrm{BIAS}_d \rangle$, are obtained: $-6 \pm 7\,\%$, $-8 \pm 9\,\%$ and $-9 \pm 9\,\%$, respectively (see Fig. 4). These similar values indicate that the BIAS is independent of CALIPSO separation with practically no increase in differences between both lidar datasets as the CALIPSO overpass increases in distance from the station. As before, these results are likely not related to spatial PSC inhomogenities.

3.2.3 Comparison analysis of particular cases

A few examples, one per year, of particular PSC events with a high/moderate CC value (see Sect. 3.1 and Table 3) are described in more detail below.

AMTD
5, 8051–8084, 2012

Figure 5 represents simultaneous 0.5-km averaged profiles of the volume linear depolarization ratio δ^{V} for MPL-4 (δ^{MPL}, filled circles) and CALIOP (δ^{CAL}, open triangles) (left), together with the corresponding BIAS (%, constraint condition shown by grey-shaded area) (right) obtained on: 30 June–1 July 2009 (top panels), 24–25 June 2010 (centre panels) and 23–24 August 2011 (bottom panels).

A good agreement is found for the PSC event observed on 30 June–1 July 2009 (see Fig. 5, top panels), as indicated by the high correlation coefficients of 0.95 and 0.91, respectively, when the CALIPSO ground-track overpass is 25.5 and 3.6 km distance from Belgrano II station (see Tables 2 and 3). δ^{V} values higher than 0.2 are obtained from around 19 km upwards and from around 18.5 up to 22 km height on 30 June and 1 July 2009, respectively. These results are also confirmed by stratospheric temperatures lower than $T^{PSC\text{-}II}$ present in the same height-range (see Fig. 2). Height-averaged percentage differences, i.e. $\langle BIAS_z \rangle$, of $+8 \pm 23$ % and -8 ± 27 % are found on 30 June and 1 July 2009, respectively.

A PSC event observed on 24 June 2010 (see Fig. 5, centre-left panel) also presents a good correlation (CC = 0.80) between MPL-4 and CALIPSO δ^{V}-profiles (CALIPSO ground-track overpass distance from the station: 2.0 km). A few hours later, on 25 June 2010 (see Fig. 5, centre-right panel), the δ^{V}-profile comparison becomes less correlated but still good enough, showing a CC = 0.64 (CALIPSO separation at 22.2 km). In particular on 24 June, $\delta^{V} > 0.2$ values are mainly found from 14 to 21.5 km height, and also at altitudes from 9 up to 12 km height corresponding to an overlapping between Cirrus clouds and PSCs. Similar features are observed on 25 June, when δ^{V} values higher than 0.2 are found from 8 up to 21 km height, where there appears a Cirrus/PSC overlapping in the height-range of 8–10 km. Regarding the particular BIAS between both MPL-4 and CALIOP δ^{V} profiles, $\langle BIAS_z \rangle$ of $+5 \pm 24$ % and $+7 \pm 30$ % are obtained on 24 and 25 June 2010, respectively.

A selected PSC event in 2011 (see Fig. 5, bottom panels) presents a nice δ^{V}-profile comparison agreement, obtaining in this case CC = 0.70 and CC = 0.58, respectively, on 23 and 24 August 2011. CALIPSO overpasses are similar to those reported in

AMTD
5, 8051–8084, 2012

both 2009 and 2010 (see Table 2). In particular on 23 August (see Fig. 5, bottom-left panel), $\delta^V > 0.2$ values are mainly found from 9 up to 16.5 km height (a Cirrus/PSC overlapping at 9–10 km height-range is present), and also at altitudes from 19 up to 24 km height. Similar features are observed on 24 August (see Fig. 5, bottom-right panel), when δ^V values higher than 0.2 are found from 9 up to 25 km height, including a Cirrus/PSC overlapping in the height-range of 9–10 km. In addition, $\langle BIAS_z \rangle$ of -8 ± 25 % and -5 ± 25 % between both lidar δ^V profiles are obtained on 23 and 24 August 2011, respectively.

These results indicate that particular PSC features are observed when individual simultaneous cases are examined, in particular for PSC events when Cirrus clouds overlapping at 8–10 km height are detected. However, in general, a high degree of agreement between the overall δ^V-profile datasets from MPL-4 and CALIOP measurements is found, with relatively low percentage differences of MPL-4 δ^V retrievals respect to CALIOP data.

4 Summary and conclusions

This study appears as a first application of the lidar depolarization technique to Antarctic PSC detection and identification by using an improved version (MPL-4) of the standard NASA/Micro Pulse Lidar. In particular, this work represents a significant advance on PSC-type discrimination studies by using MPL-4 δ^V data.

Calibration parameters for suitable MPL-4 δ^V retrievals have been calculated from MPL-4 measurements, and the calibrated δ^V profiles have been compared with simultaneous CALIPSO data as a reference during 2009–2011 austral winters, from May to September periods, over Belgrano II station (Antarctica). Two analysis procedures for δ^V profile comparisons have been presented.

The results indicate a good correlation between both ground-based and space-borne PSC volume linear depolarization ratio δ^V datasets once the MPL-4 depolarization

AMTD
5, 8051–8084, 2012

calibration parameters are applied. Indeed, 54 % out of all the cases present CC values higher than 0.5, at least in the altitude-range from 5 to 20 km, with the correlation decreasing at altitudes higher than 25 km. These results represent a relatively good agreement between MPL-4 and CALIOP profiles of the volume linear depolarization ratio δ^{V} for PSC events.

The comparison parameter, BIAS, seems to be a less robust indicator of the degree of agreement for lidar δ^{V} datasets, since less than a half of the cases fulfil the selected constraint condition ($-50\% < \mathrm{BIAS} < +50\%$), showing a large data dispersion with percentage differences between lidar datasets higher than ±50 %. However, with respect to constrained BIAS values, differences between δ^{MPL} and δ^{CAL} are no higher than an 11 % (absolute value) in comparison with CALIOP values in the worse case (in 2011). Moreover, a predominance of negative BIAS is observed, indicating a δ^{MPL} underestimation with respect to δ^{CAL}.

Moreover, the δ^{V} agreement between both lidar datasets is relatively independent of the CALIPSO ground-track overpass distance from the Belgrano II station, as shown by both the correlation (CC) and percentages differences (BIAS) obtained. Consequently, discrepancies between both the δ^{V} datasets are not dominated by spatial PSC inhomogeneities. Therefore, further work based on the correlation between the PSC field and stratospheric temperatures is on-going in order to clarify the observed discrepancies.

In addition, a detailed 3-yr statistical analysis of PSC occurrence over Belgrano II station in terms of both the backscattering, R, and volume linear depolarization, δ^{V}, ratios from MPL-4 measurements, is underway to complete these studies. This will include a PSC-type discrimination assessment over Belgrano II station and well inside the Antarctic polar vortex. These results are useful for PSC detection and classification in both polar regions by using this kind of micro pulse lidar that operates in full-time continuous mode, providing a more complete evolution of the PSC field on a daily basis.

AMTD
5, 8051–8084, 2012

Acknowledgements. This work has been supported by the Spanish Ministry for Science and Innovation (MICINN) under grant CGL2010-20353 (project VIOLIN) and the Spanish Ministry of Education (MEC) fellowship EX2009-0700. CALIPSO data were obtained from the NASA Langley Research Center Atmospheric Science Data Center. Authors specially thank the DNA/IAA teams at Belgrano II station for their valuable assistance and support in the lidar and radiosounding measurements.

References

Adriani, A., Massoli, P., Di Donfrancesco, G., Cairo, F., Moriconi, M. L., and Snels, M.: Climatology of polar stratospheric clouds based on lidar observations from 1993 to 2001 over McMurdo station, Antarctica, J. Geophys. Res., 109, D24211, doi:10.1029/2004JD004800, 2004.

Álvarez, J. M., Vaughan, M. A., Hostetler, C. A., Hunt, W. H., and Winker, D. M.: Calibration technique for polarization-sensitive lidars, J. Atmos. Ocean. Technol., 23, 683–699, 2006.

Cairo, F., Di Donfrancesco, G., Adriani, A., Pulvirenti, L., and Fierli, F.: Comparison of various depolarization parameters measured by lidar, Appl. Opt., 38, 4425–4432, 1999.

Campbell, J. R. and Sassen, K.: Polar stratospheric clouds at the South Pole from five years of continuous lidar data: macrophysical, optical and thermodynamic properties, J. Geophys. Res., 113, D20204, doi:10.1029/2007JD009680, 2008.

Campbell, J. R., Hlavka, D. L., Welton, E. J., Flynn, C. J., Turner, D. D., Spinhirne, J. D., Scott, V. S., and Hwang, I. H.: Full-time, eye-safe cloud and aerosol lidar observation at Atmospheric Radiation Measurement program sites: instruments and data processing, J. Atmos. Ocean. Technol., 19, 431–442, 2002.

Córdoba-Jabonero, C., Gil, M., Yela, M., Maturilli, M., and Neuber, R.: Polar Stratospheric Cloud observations in the 2006/07 Arctic winter by using an improved Micro Pulse Lidar, J. Atmos. Ocean. Technol., 26, 2136–2148, 2009.

Fernald, F. G.: Analysis of atmospheric lidar observations: some comments, Appl. Opt., 23, 652–653, 1984.

Hanson, D. R. and Mauersberger, K.: Laboratory studies of the nitric acid trihydrate: implications for the south polar stratosphere, Geophys. Res. Lett., 15, 855–858, 1988.

AMTD

5, 8051–8084, 2012

Hostetler, C. A., Liu, Z., Reagan, J., Vaughan, M., Winker, D., Osborn, M., Hunt, W. H., Powell, K. A., and Trepte, C.: CALIOP Algorithm Theoretical Basis Document, Calibration and level 1 Data Products, PC-SCI-201, NASA Langley Research Center, Hampton, VA 23681, USA, 2006.

Hunt, W. H., Winker, D. M., Vaughan, M. A., Powell, K. A., Lucker, P. L., and Weimer, C.: CALIPSO lidar description and performance assessment, J. Atmos. Ocean. Technol., 26, 1214–1228, 2009.

Innis, J. L. and Klekociuk, A. R.: Planetary wave and gravity wave influence on the occurrence of polar stratospheric clouds over Davis Station, Antarctica, seen in lidar and radiosonde observations, J. Geophys. Res., 111, D22102, doi:10.1029/2006JD007629, 2006.

Klett, J. D.: Stable analytic inversion solution for processing lidar returns, Appl. Opt., 20, 211–220, 1981.

Maturilli, M., Neuber, R., Massoli, P., Cairo, F., Adriani, A., Moriconi, M. L., and Di Donfrancesco, G.: Differences in Arctic and Antarctic PSC occurrence as observed by lidar in Ny-Ålesund (79° N, 12° E) and McMurdo (78° S, 167° E), Atmos. Chem. Phys., 5, 2081–2090, doi:10.5194/acp-5-2081-2005, 2005.

Pal, S. R. and Carswell, A. I.: Polarization properties of lidar backscattering from clouds, Appl. Opt., 12, 1530–1535, 1973.

Parrondo, M. C., Yela, M., Gil, M., von der Gathen, P., and Ochoa, H.: Mid-winter lower stratosphere temperatures in the Antarctic vortex: comparison between observations and ECMWF and NCEP operational models, Atmos. Chem. Phys., 7, 435–441, doi:10.5194/acp-7-435-2007, 2007.

Pitts, M. C., Thomason, L. W., Poole, L. R., and Winker, D. M.: Characterization of Polar Stratospheric Clouds with spaceborne lidar: CALIPSO and the 2006 Antarctic season, Atmos. Chem. Phys., 7, 5207–5228, doi:10.5194/acp-7-5207-2007, 2007.

Pitts, M. C., Poole, L. R., and Thomason, L. W.: CALIPSO polar stratospheric cloud observations: second-generation detection algorithm and composition discrimination, Atmos. Chem. Phys., 9, 7577–7589, doi:10.5194/acp-9-7577-2009, 2009.

Pitts, M. C., Poole, L. R., Dörnbrack, A., and Thomason, L. W.: The 2009–2010 Arctic polar stratospheric cloud season: a CALIPSO perspective, Atmos. Chem. Phys., 11, 2161–2177, doi:10.5194/acp-11-2161-2011, 2011.

Powell, K., Vaughan, M., Winker, D., Lee, K.-P., Pitts, M., Trepte, C., Detweiler, P., Hunt, W., Lambeth, J., Lucker, P., Murray, T., Hagolle, O., Lifermann, A., Faivre, M., Garnier, A., and Pelon,

AMTD
5, 8051–8084, 2012

J.: Cloud – Aerosol LIDAR Infrared Pathfinder Satellite Observations (CALIPSO), Data Management System, Data Products Catalog, Document No: PC-SCI-503, Release 3.2, August 2010, NASA Langley Research Center, Hampton, Virginia, USA, 2010.
Rubin, M. J.: Seasonal variations of the Antarctic tropopause, Met., 10, 127–134, 1953.
Santacesaria, V., MacKenzie, A. R., and Stefanutti, L.: A climatological study of polar stratospheric clouds (1989–1997) from LIDAR measurements over Dumont d'Urville (Antarctica), Tellus, 53B, 306–321, 2001.
Sassen, K.: Polarization in Lidar, in: Lidar: Range-Resolved Optical Remote Sensing of the Atmosphere, edited by: Weitkamp, C., Optical Sci., Springer Ser., Singapore, 2005.
Sassen, K. and Benson, S.: A midlatitude cirrus cloud climatology from the Facility for Atmospheric Remote Sensing. Part II: Microphysical properties derived from lidar depolarization, J. Atmos. Sci., 58, 2103–2112, 2001.
Schotland, R. M., Sassen, K., and Stone, R.: Observations by lidar of linear depolarization ratios by hydrometeors, J. Appl. Meteorol., 10, 1011–1017, 1971.
Shibata, T., Sato, K., Kobayashi, H., Yabuki, M., and Shiobara, M.: Antarctic polar stratospheric clouds under temperature perturbation by nonorographic inertia gravity waves observed by micropulse lidar at Syowa Station, J. Geophys. Res., 108, 4105, doi:10.1029/2002JD002713, 2003.
Solomon, S.: Stratospheric ozone depletion: a review of concepts and history, Rev. Geophys., 37, 275–316, 1999.
Toon, O. B., Browell, E. V., Kinne, S., and Jordan, J.: An analysis of lidar observations of polar stratospheric clouds, Geophys. Res. Lett., 17, 393–396, 1990.
Waugh, D. W. and Polvani, L. M.: Stratospheric polar vortices, in: The Stratosphere: Dynamics, Chemistry, and Transport, Geophys. Monogr. Ser., 190, edited by: Polvani, L. M., Sobel, A. H., and Waugh, D. W., AGU, Washington, D. C., 43–57, 2010.
Winker, D. M., Hunt, W. H., and McGill, M. J.: Initial performance assessment of CALIOP, Geophys. Res. Lett., 34, L19803, doi:10.1029/2007GL030135, 2007.

AMTD
5, 8051–8084, 2012

Table 1. Mean χ values together with their SD (%SD) and the number of profiles used.

Year	χ	SD (%SD)	Number of profiles
2009	−0.053	0.005 (10.4)	271
2010	−0.059	0.006 (10.8)	275
2011	−0.053	0.008 (15.4)	232
Mean/Total	−0.055	0.003 (5.2)	778

AMTD
5, 8051–8084, 2012

Table 2. Simultaneous PSC events between MPL-4 and CALIOP measurements: Date and time of the CALIPSO overpass together with its ground-track distance from Belgrano II station. Closest local radiosounding used for MPL-4 retrievals to that PSC occurrence is also shown.

Event	Date	Time (UTC)	Distance (km)	Local radio-sounding date
		2009 (15 cases)		
1	15/06	01:19	3.3	17/06
2	28/06	19:01	26.9	29/06
	29/06	01:31	50.1	
	30/06	18:48	25.5	
	01/07	01:18	3.6	
3	30/07	19:00	25.6	29/07
	31/07	01:30	48.9	
	01/08	18:47[a]	27.0	
	02/08	01:18	4.7	
4	25/08	01:23	22.2	27/08
	27/08	01:11	30.1	
5	25/09	18:53	0.3	23/09
	26/09	01:23	23.3	
	27/09	18:40	54.0	
	28/09	01:11	29.0	
		2010 (18 cases)		
6	08/06	18:51	1.6	02/06
	09/06	01:21	22.4	
	10/06	18:38	55.5	
	11/06	01:09	29.8	
7	24/06	18:50	2.0	30/06
	25/06	01:21	22.2	
	26/06	18:38	55.7	
	27/06	01:09	29.9	

AMTD
5, 8051–8084, 2012

Table 2. (Continued).

Event	Date	Time (UTC)	Distance (km)	Local radio-sounding date
8	01/07	18:57	24.4	07/07
	02/07	01:27	49.7	
	03/07	18:44[a]	28.0	
	04/07	01:15[a]	3.8	
9	12/07	18:38	54.9	07/07
	13/07	01:09	29.0	
10	27/08	18:50	1.0	25/08
	28/08	01:21	24.1	
11	19/09	18:56	23.5	22/09
	20/09	01:26	50.2	
2011 (15 cases)				
12	28/05	18:37	56.8	25/05
	29/05	01:08	29.5	
13	03/06	01:26	50.3	08/06
14	06/07	18:43[a]	29.3	06/07
	07/07	01:14	3.1	
15	15/07	18:37	56.7	20/07
	16/07	01:07	28.9	
16	29/07	18:49	2.5	27/07
	30/07	01:20	23.9	
17	14/08	18:49	2.7	17/08
	15/08	01:20	24.0	
18	21/08	18:55	23.1	24/08
	22/08	01:26	50.8	
	23/08	18:43	29.4	
	24/08	01:13	2.7	

[a] Available, but not coincident in time with CALIPSO overpass, MPL-4 profile used instead for retrieval calculations.

AMTD
5, 8051–8084, 2012

Table 3. Correlation coefficient (CC) for five selected height intervals.

Date	5–10 km	5–15 km	5–20 km	5–25 km	5–30 km
			2009 (15 cases)		
15/06	0.32	0.40	0.35	0.18	0.47
28/06	−0.06	−0.07	0.46	0.12	−0.14
29/06	−0.31	−0.15	0.07	0.82	0.60
30/06*	0.17	−0.09	0.71	0.95	0.58
01/07*	0.46	0.05	0.84	0.91	0.67
30/07	0.02	0.76	0.75	0.85	0.67
31/07	−0.09	0.66	0.54	0.50	0.39
01/08	0.74	0.47	0.54	0.59	0.68
02/08	−0.12	0.69	0.49	0.37	0.06
25/08	−0.18	0.75	0.71	0.62	0.43
27/08	0.52	0.36	0.33	0.14	0.39
25/09	−0.26	−0.20	−0.15	−0.07	−0.10
26/09	0.33	0.44	0.12	−0.14	0.64
27/09	0.34	0.70	0.24	0.28	0.07
28/09	0.58	0.94	0.87	0.55	0.19
			2010 (18 cases)		
08/06	0.82	0.82	0.61	0.54	0.36
09/06	0.55	0.56	0.56	0.49	0.11
10/06	0.00	0.58	0.11	0.00	0.35
11/06	−0.05	0.49	0.50	0.29	0.18
24/06*	0.95	0.88	0.89	0.80	0.64
25/06*	0.94	0.81	0.74	0.64	0.45
26/06	0.47	0.56	0.41	0.51	0.38
27/06	0.42	0.40	0.41	0.44	0.14

* Particular analysed cases are marked by asterisks.

AMTD
5, 8051–8084, 2012

PSC depolarization ratio: MPL vs. CALIOP comparison

C. Córdoba-Jabonero et al.

Table 3. (Continued).

Date	5–10 km	5–15 km	5–20 km	5–25 km	5–30 km
01/07	0.81	0.59	0.25	0.26	0.45
02/07	0.57	0.64	0.54	0.52	0.12
03/07	0.35	−0.28	0.30	0.28	0.33
04/07	−0.17	−0.19	−0.16	−0.28	0.09
12/07	0.34	0.35	0.22	0.26	0.18
13/07	0.68	0.61	0.51	−0.03	−0.03
27/08	0.80	0.21	0.57	0.07	0.01
28/08	−0.20	0.75	0.73	0.24	0.54
19/09	−0.32	−0.06	0.10	0.03	−0.17
20/09	−0.22	0.13	0.29	0.24	0.20
2011 (15 cases)					
28/05	0.42	0.11	−0.03	−0.14	0.33
29/05	0.35	0.01	0.47	−0.11	0.38
03/06	−0.19	−0.16	0.27	−0.17	0.41
06/07	−0.16	0.76	0.52	0.49	0.07
07/07	0.64	0.83	0.90	0.65	0.22
15/07	0.19	0.40	0.41	0.36	0.27
16/07	0.66	0.78	0.38	0.28	0.11
29/07	0.79	0.68	0.66	0.45	0.29
30/07	0.24	0.34	0.70	0.50	0.32
14/08	0.54	0.62	0.58	0.09	0.25
15/08	0.00	0.24	0.21	−0.20	0.29
21/08	−0.21	0.33	0.33	0.41	0.04
22/08	0.32	0.56	0.61	0.39	0.39
23/08*	0.65	0.77	0.70	0.44	0.27
24/08*	0.89	0.80	0.58	0.51	0.34

* Particular analysed cases are marked by asterisks.

AMTD
5, 8051–8084, 2012

Table 4. Calculated height-averaged BIAS, $\langle BIAS_z \rangle$, and their SD together with the number of data points (in % respect to the total "valid" data points N) fulfilling the constraint condition (in brackets).

Date	N (% out of 50)	N^{BIAS} (%) (−50 % < BIAS < +50 %)	$\langle BIAS_z \rangle$ (%)	SD (%)
		2009 (15 cases)		
15/06	84	28.6	4	32
28/06	74	35.1	−19	19
29/06	88	25.0	−13	27
30/06*	86	39.5	8	23
01/07*	86	39.5	−8	27
30/07	90	44.4	5	26
31/07	74	32.4	−6	31
01/08	82	34.1	−16	31
02/08	50	60.0	−2	21
25/08	88	40.9	−12	21
27/08	90	33.3	−11	28
25/09	88	31.8	−3	31
26/09	88	25.0	−19	17
27/09	84	33.3	−12	28
28/09	76	18.4	−6	31
		2010 (18 cases)		
08/06	56	35.7	−10	33
09/06	44	31.8	−16	28
10/06	36	33.3	−14	24
11/06	82	36.6	−16	27
24/06*	82	48.8	5	24
25/06*	90	46.7	7	30
26/06	84	38.1	8	24
27/06	84	33.3	−2	27

* Particular analysed cases are marked by asterisks.

AMTD
5, 8051–8084, 2012

Table 4. (Continued).

Date	N (% out of 50)	N^{BIAS} (%) (−50 % < BIAS < +50 %)	$\langle BIAS_z \rangle$ (%)	SD (%)
01/07	90	24.4	−14	27
02/07	72	47.2	−6	27
03/07	58	17.2	−18	18
04/07	44	50.0	−12	23
12/07	94	38.3	2	28
13/07	90	55.6	0	26
27/08	66	33.3	−10	15
28/08	80	30.0	−2	29
19/09	88	18.2	−4	28
20/09	82	31.7	−8	27
2011 (15 cases)				
28/05	94	17.0	−28	22
29/05	82	26.8	−2	31
03/06	60	33.3	−8	22
06/07	88	40.9	−8	26
07/07	90	35.6	−19	30
15/07	80	47.5	−2	30
16/07	68	52.9	−8	27
29/07	86	48.8	−15	23
30/07	92	28.3	−21	30
14/08	74	35.1	1	26
15/08	78	38.5	−23	23
21/08	86	58.1	2	22
22/08	96	56.3	−15	24
23/08*	100	62.0	−8	25
24/08*	84	54.8	−5	25

* Particular analysed cases are marked by asterisks.

AMTD
5, 8051–8084, 2012

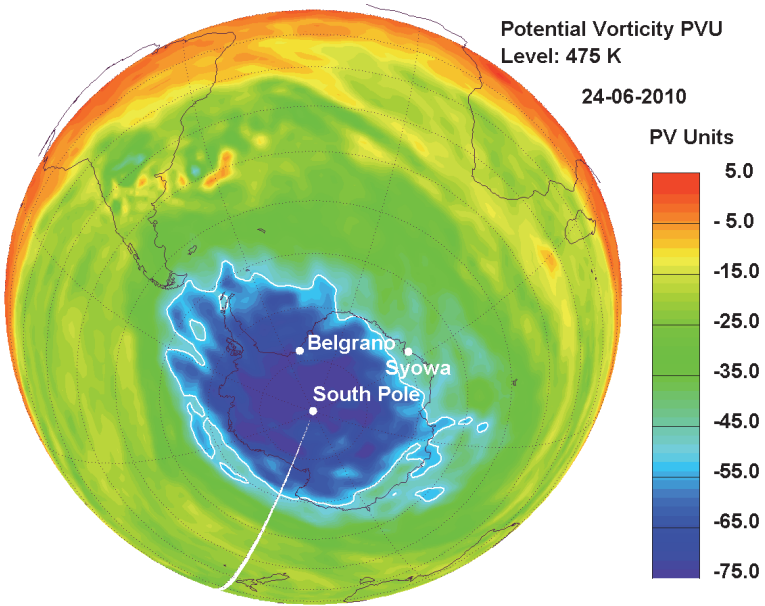

Fig. 1. Stable polar vortex over Antarctica represented by the potential vorticity (PV) at 475 K-level on 24 June 2010. The white line indicates the edge of the polar vortex. Also shown are the location of Belgrano II station (Argentina, 77.9° S 34.6° W) together with Syowa (Japan, 69.0° S 39.5° E), which is outside the polar vortex edge, and South Pole/Amundsen-Scott (USA, 89.98° S 24.8° E) stations.

AMTD
5, 8051–8084, 2012

PSC depolarization ratio: MPL vs. CALIOP comparison

C. Córdoba-Jabonero et al.

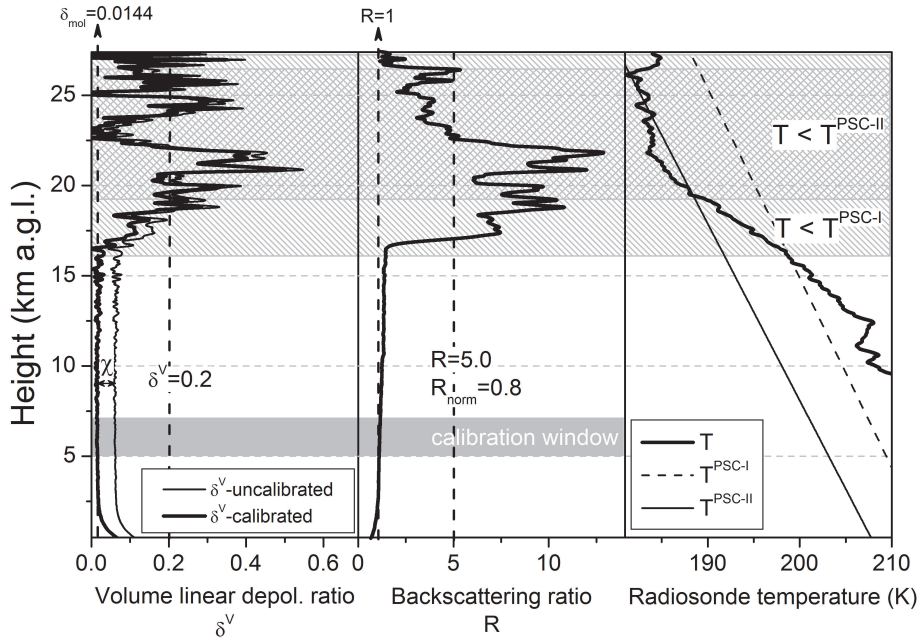

Fig. 2. An example of calibration of the volume linear depolarization ratio δ^V. From left to right: 1h-averaged (01:00–02:00 UTC) δ^V profile on 1 July 2009, once calibrated (thick solid line) and before calibration (thin solid line); the corresponding backscattering ratio R profile; and the closest available temperature radiosounding on 29 June 2009 at 11:00 UTC together with the threshold temperatures for PSC-I ($T^{PSC\text{-}I}$, dashed line) and PSC-II ($T^{PSC\text{-}II}$, solid line) formation with 5-ppmv H_2O and 10-ppbv HNO_3 as a reference (Maturilli et al., 2005). CALIPSO ground-track distance is 3.6 km far from the Belgrano II station on this day.

AMTD
5, 8051–8084, 2012

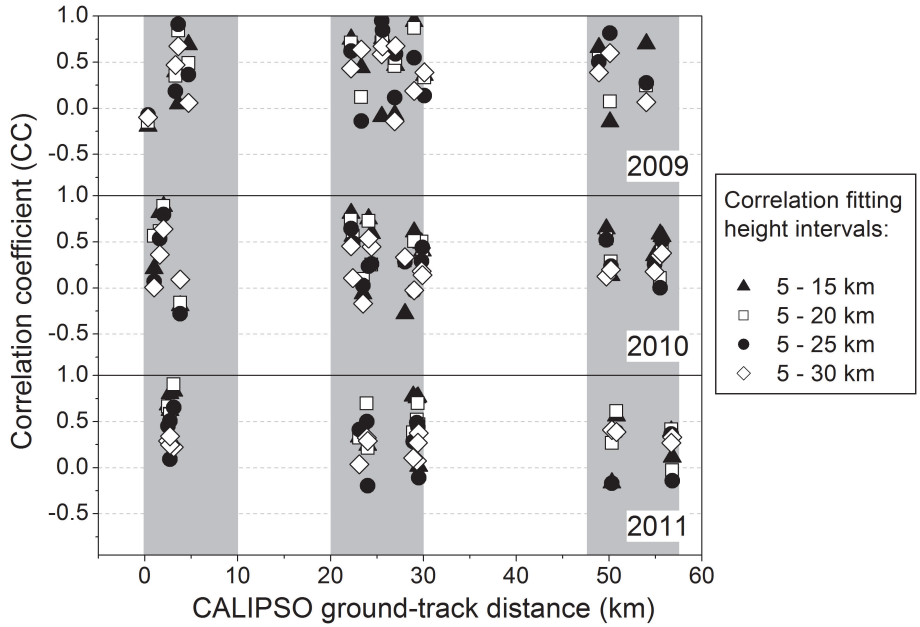

Fig. 3. Correlation coefficient (CC) variation in relation with the CALIPSO ground-track distance from Belgrano II station during 2009 (top), 2010 (centre) and 2011 (bottom) wintertime periods for four fitting height intervals (see legend).

AMTD
5, 8051–8084, 2012

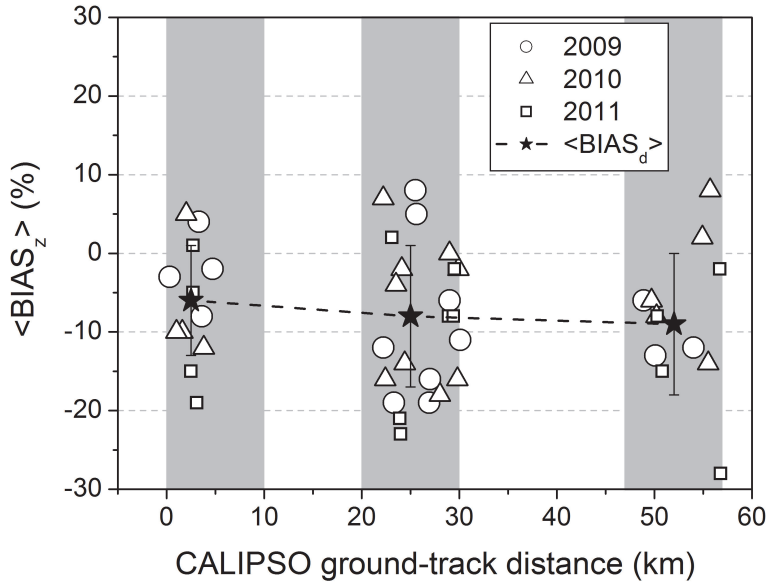

Fig. 4. Height-averaged BIAS, $\langle BIAS_z \rangle$, in relation with the CALIPSO ground-track distance from Belgrano II station for 2009 (circles), 2010 (triangles) and 2011 (squares) wintertime periods. Those averaged values on each predominant separation distance $\langle BIAS_d \rangle$ (SD is marked by error bars) are also shown (black stars).

AMTD
5, 8051–8084, 2012

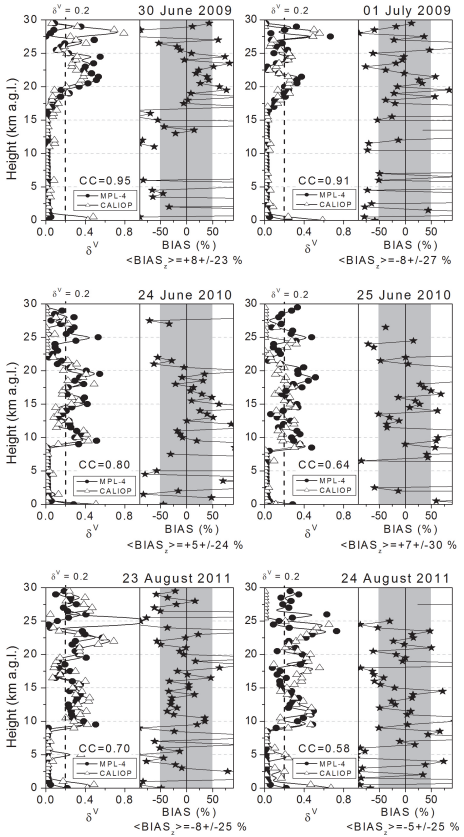

Fig. 5. Simultaneous 0.5-km averaged profiles of the volume linear depolarization ratio δ^V for MPL-4 (full dots) and CALIOP (open triangles) (left), and the BIAS (%, constraint condition shown by grey-shaded area) (right) for PSC events observed on: 30 June–1 July 2009 (top panels), 24–25 June 2010 (centre panels) and 23–24 August 2011 (bottom panels). Height-averaged BIAS, $\langle BIAS_z \rangle$, and their SD values, are also shown in each case (see Table 4).

AMTD
5, 8051–8084, 2012

PSC depolarization ratio: MPL vs. CALIOP comparison

C. Córdoba-Jabonero et al.